PAPER

Check for updates

Synthesis of W-modified CeO_2/ZrO_2 catalysts for selective catalytic reduction of NO with NH_3†

Chenglong Li,[a] Zhitao Han, ✶[a] Yuqing Hu,[a] Tingjun Liu[a] and Xinxiang Pan[ab]

In this paper, a series of tungsten–zirconium mixed binary oxides (denoted as W_mZrO_x) were synthesized via co-precipitation as supports to prepare $Ce_{0.4}/W_mZrO_x$ catalysts through an impregnation method. The promoting effect of W doping in ZrO_2 on selective catalytic reduction (SCR) performance of $Ce_{0.4}/ZrO_2$ catalysts was investigated. The results demonstrated that addition of W in ZrO_2 could remarkably enhance the catalytic performance of $Ce_{0.4}/ZrO_2$ catalysts in a broad temperature range. Especially when the W/Zr molar ratio was 0.1, the $Ce_{0.4}/W_{0.1}ZrO_x$ catalyst exhibited the widest active temperature window of 226–446 °C (NO_x conversion rate > 80%) and its N_2 selectivity was almost 100% in the temperature of 150–450 °C. Moreover, the $Ce_{0.4}/W_{0.1}ZrO_x$ catalyst also exhibited good SO_2 tolerance, which could maintain more than 94% of NO_x conversion efficiency after being exposed to a 100 ppm SO_2 atmosphere for 18 h. Various characterization results manifested that a proper amount of W doping in ZrO_2 was not only beneficial to enlarge the specific surface area of the catalyst, but also inhibited the growth of fluorite structure CeO_2, which were in favor of CeO_2 dispersion on the support. The presence of W was conducive to the growth of a stable tetragonal phase crystal of ZrO_2 support, and a part of W and Zr combined to form $W–Zr–O_x$ solid super acid. Both of them resulted in abundant Lewis acid sites and Brønsted acid sites, enhancing the total surface acidity, thus significantly improving NH_3 species adsorption on the surface of the $Ce_{0.4}/W_{0.1}ZrO_x$ catalyst. Furthermore, the promoting effect of adding W on SCR performance was also related to the improved redox capability, higher $Ce^{3+}/(Ce^{3+} + Ce^{4+})$ ratio and abundant surface chemisorbed oxygen species. The in situ DRIFTS results indicated that nitrate species adsorbed on the surface of the $Ce_{0.4}/W_{0.1}ZrO_x$ catalyst could react with NH_3 due to the activation of W. Therefore, the reaction pathway over the $Ce_{0.4}/W_{0.1}ZrO_x$ catalyst followed both Eley–Rideal (E–R) and Langmuir–Hinshelwood (L–H) mechanisms at 250 °C.

1. Introduction

Selective catalytic reduction of nitrogen oxides with NH_3 (NH_3-SCR) has been widely employed for NO_x abatement applications in stationary and mobile sources.[1,2] During the past decades, V_2O_5–WO_3 (or MoO_3)/TiO_2 had been considered the most pervasive and efficient SCR catalysts.[3] However, these catalysts still suffer from some inevitable shortcomings in practical application, such as a narrow operation temperature window (300–400 °C), toxicity of vanadium pentoxide and low N_2 selectivity at high temperatures.[4] Given these disadvantages, great efforts have been made to develop environmentally friendly catalysts with a wide temperature window and high N_2 selectivity.

[a]Marine Engineering College, Dalian Maritime University, No.1, Linghai Road, Dalian 116026, China. E-mail: hanzt@dlmu.edu.cn

[b]School of Electronic and Information Technology, Guangdong Ocean University, Zhanjiang 524088, China

† Electronic supplementary information (ESI) available. See https://doi.org/10.1039/d2ra04862k

In recent years, some non-toxic SCR catalysts such as MnO_x, Fe_2O_3, CuO and CeO_2, have been extensively investigated in order to substitute vanadium-based catalysts.[5–8] Among them, cerium-based NH_3-SCR catalysts have attracted a lot of researchers' interest due to their high oxygen storage/release capacity and remarkable redox properties, which are significant to the oxidation of NO_x and the acceleration of NH_3-SCR reactions.[9] However, pure CeO_2 catalysts exhibit poor thermal stability and are easy to sinter at high temperature. In addition, the high active surface oxygen of a pure CeO_2 catalyst results in NH_3 oxidation on the catalyst surface, especially at high temperature, leading to a decrease in SCR activity.[8,10] It is generally believed that acid sites are beneficial to suppress NH_3 oxidation and promoting NH_3 adsorption on the catalyst surface. Therefore, it should be feasible to enhance acid sites to improve NO_x conversion and N_2 selectivity of a CeO_2 catalyst.[11,12]

Zirconia (ZrO_2) is an acid-based amphoteric oxide with excellent redox capability and high refractory property. Previous studies reported that the addition of ZrO_2 to CeO_2 led to an improvement on thermal stability and oxygen storage capacity.[13] ZrO_2-supported CeO_2 catalysts exhibited good oxygen

storage capacity and highly refractory property at the same time. It can utilize the large surface area of ZrO_2 to promote the dispersion of CeO_2 on catalyst surface. Previous studies showed that CeO_2/ZrO_2 catalysts possessed excellent NH_3-SCR activity at medium temperature.[14,15] Nonetheless, the low-temperature activity and SO_2 tolerance of CeO_2/ZrO_2 catalyst are still not very satisfactory, which hinders their industrial application.

As an important additive in traditional V-based catalysts, WO_3 has been recognized as an excellent "chemical" and "structural" promoter to improve SCR performance obviously.[16] Previous studies have shown that the addition of WO_3 could enhance the adsorption and activation of NH_3 by increasing the surface acidity of the catalysts, which was beneficial to the improvement of NH_3-SCR activity.[17,18] Recently, Fang *et al.* prepared $WO_3/Ce_{0.65}Zr_{0.35}O_2$ catalyst by co-precipitation and impregnation method, it could obtain an excellent NH_3-SCR performance at 250–450 °C.[19] Väliheikki *et al.* have proven that the $WO_3/Ce_{0.85}Zr_{0.15}O_2$ catalyst exhibited high SO_2 and H_2O resistance in the temperature range of 300–500 °C.[20] In these studies, WO_3 was usually used as a surface modifier to modify the catalyst surface. However, there are few reports about the incorporation of W into ZrO_2 to form binary metal oxide support for NH_3-SCR. Chen *et al.* reported that, the addition of W in ZrO_2 could enhance the total acidity and redox properties by forming $W–Zr–O_x$, which would greatly promote the SCR performance.[21,22] The authors considered that $W–Zr–O_x$ solid super acid could be used as SCR support with a high surface area, which might enhance the catalytic activity of Ce/Zr catalysts greatly.

In this work, we focused on the effects of W doping in ZrO_2 on SCR performance of Ce/ZrO_2 catalyst. A series of $Ce/WZrO_x$ catalysts were prepared by successive co-precipitation and impregnation methods. Catalytic performance tests showed that $Ce/WZrO_x$ catalysts exhibited a much higher NO_x removal efficiency than that of Ce/ZrO_2 catalyst. Further, the effects of W doping in ZrO_2 were investigated in detail by using N_2 physisorption, XRD, Raman, SEM, TEM, XPS, H_2-TPR, NH_3-TPD and *in situ* DRIFTS. Finally, the possible reaction mechanisms were also discussed to gain insights into the effect of $WZrO_x$ solid super acid support on SCR reaction pathways.

2. Experimental

2.1 Catalyst preparation

A series of tungsten–zirconium oxides with various molar ratios of W/Zr were prepared by using the co-precipitation method. The typical synthesis process was as follows: a proper amount of $Zr(NO_3)_4 \cdot 5H_2O$ and $(NH_4)_{10}H_2(W_2O_7)_6 \cdot xH_2O$ were dissolved in deionized water. Then the mixed solution was heated to 40 °C and held for 2 h under continuous magnetic stirring. Next, ammonia solution (25 wt%) was added dropwise to the above solution with vigorous stirring to adjust the solution pH to 10. The obtained precipitate was naturally cooled down to room temperature for 5 h and then filtered, and washed with deionized water until pH changed little. Afterwards, the precipitate was washed with anhydrous ethanol, and dried at 80 °C overnight. The collected solid was calcined at 550 °C in air for 3 h,

and finally grounded into a fine powder. The prepared tungsten–zirconium mixed oxides were denoted as W_mZrO_x, where m represented the molar ratio of W/Zr ($m = 0.025, 0.05, 0.1, 0.2$). Pristine ZrO_2 was also prepared for reference by using the precipitation method.

Both $Ce_{0.4}/ZrO_2$ and $Ce_{0.4}/W_mZrO_x$ catalysts were prepared by the impregnation method, where 0.4 represented the molar ratio of Ce/Zr. Firstly, a certain amount of $Ce(NO_3)_3 \cdot 6H_2O$ was dissolved in deionized water. Then a desired amount of ZrO_2 or W_mZrO_x powder was impregnated in the solution with strong stirring for 0.5 h. Next, the mixture continued to be stirred sufficiently at 80 °C in a water bath to evaporate the solvent. The solid was dried at 100 °C for 12 h, and calcined at 500 °C for 3 h in air. Finally, all catalysts were crushed and sieved to 40–60 mesh for testing.

2.2 Catalyst activity test

The SCR activity tests of these prepared catalysts were carried out in a fixed-bed quartz reactor (I.D. 6 mm) at atmospheric pressure with a catalyst dosage of 0.5 mL (40–60 mesh). SCR activity measurements were operated in a temperature range of 150–450 °C. The simulated gas consisted of 500 ppm NO, 500 ppm NH_3, 5 vol% O_2, 100 ppm SO_2 (when used) and N_2 as balance gas with a total flow rate of 500 mL min^{-1}. The corresponding gas hourly space velocity (GHSV) was 60 000 h^{-1}. The outlet concentrations of NO, NO_2, NH_3 and N_2O were monitored by an FTIR spectrometer (Antaris IGS, ThermoFisher Scientific) equipped with a heated low-volume multiple-path gas cell (2 m) and an MCT detector cooled by liquid nitrogen. Here NO_x referred to the sum of NO and NO_2. NO_x conversion efficiency and N_2 selectivity were calculated as follows:

$$NO_x \text{ conversion } (\%) = \frac{[NO_x]_{in} - [NO_x]_{out}}{[NO_x]_{in}} \times 100\% \quad (1)$$

$$N_2 \text{ selectivity } (\%) = \left(1 - \frac{2[N_2O]_{out}}{[NO_x]_{in} - [NO_x]_{out} + [NH_3]_{in} - [NH_3]_{out}}\right) \times 100\% \quad (2)$$

2.3 Catalyst characterization

The textural properties of the prepared samples were measured using N_2 physisorption (ASAP 2020 PLUS, Micromeritics). The powder X-ray diffraction (XRD) patterns were performed on a diffractometer (TTRAX III, Rigaku, Japan) with a Cu-Kα radiation source ($\lambda = 0.15406$ nm) under 40 kV and 30 Ma. The Raman spectra of samples were carried out at a Raman Spectrometer (RM2000, Renishaw), using an Ar ion laser (532 nm) as the excitation source. The morphology of the samples was characterized by scanning electron microscopic (SEM, Tescan Mira4). The transmission electron microscopic (TEM) images were performed on FEI Talos F200X and the chemical analysis was obtained by energy dispersive X-ray spectrometer (EDS, Oxford Ultim Max65). X-ray photoelectron spectroscopy (XPS) measurement was obtained on a surface analysis photoelectron spectrometer (ESCALAB 250Xi, ThermoFisher Scientific) using

Al Kα as a radiation source. Temperature programmed reduction with H_2 (H_2-TPR) experiments were operated on a chemisorption analyzer (Autochem II 2920, Micromeritics). Temperature programmed desorption of NH_3 (NH_3-TPD) experiments were operated on a chemisorption analyzer (Autochem II 2920, Micromeritics). *In situ* DRIFTS measurements were carried out by an FTIR spectrometer (Nicolet iS50, ThermoFisher Scientific) equipped with an MCT/A detector. The spectral resolution was 4 cm^{-1} with co-addiction 64 scans.

3. Results and discussion

3.1 SCR performance

The catalytic performance of the prepared catalysts for NH_3-SCR of NO_x in the temperature range of 150–450 °C was tested, and the results were displayed in Fig. 1. It could be seen from Fig. 1(a) that W-doped ZrO_2 supports imposed significant impacts on SCR catalytic activities of $Ce_{0.4}/ZrO_2$ catalysts. Without W doping, $Ce_{0.4}/ZrO_2$ catalyst showed rather poor SCR activity in the whole temperature region with the maximum NO_x conversion of only about 56% at 370 °C, which was in accordance with our previous study.[15] In contrast, $Ce_{0.4}/W_mZrO_x$ catalysts exhibited much better catalytic activity in the test temperature range. With the increase of W/Zr molar ratio from 0.025 to 0.1, the promotional effect of W on SCR activity was observed over W-containing catalysts with dramatically increasing NO_x conversion and broadened operation temperature windows. However, further increasing W/Zr molar ratio to 0.2, SCR performance of $Ce_{0.4}/W_{0.2}ZrO_x$ catalysts deteriorated obviously in the whole operating temperature, and NO_x conversion efficiency was only 41% at 226 °C. After all, $Ce_{0.4}/W_{0.1}ZrO_x$ catalyst possessed the largest active temperature window (NO_x conversion rate > 80%) of 226–446 °C under GHSV of 60 000 h^{-1}. Fig. 1(b) showed the N_2 selectivity of $Ce_{0.4}/ZrO_2$ and $Ce_{0.4}/W_mZrO_x$ catalysts. It could be seen that N_2 selectivity over $Ce_{0.4}/ZrO_2$ catalyst began to decline slowly when the reaction temperature was above 375 °C, and reduced to 95% at 450 °C. In contrast, all $Ce_{0.4}/W_mZrO_x$ catalysts exhibited superior N_2 selectivity. It was close to 100% in the whole temperature range. The above results demonstrated that the doping of W in ZrO_2 supports could remarkably improve NH_3-SCR performance of Ce/Zr catalysts. Since the comprehensive performance of $Ce_{0.4}/W_{0.1}ZrO_x$ catalyst was obviously better than other catalysts, comparative investigations between $Ce_{0.4}/ZrO_2$ and $Ce_{0.4}/W_{0.1}ZrO_x$ catalysts were conducted to elucidate the effect of W–Zr binary metal oxide support on NH_3-SCR performance.

It is well known that the common catalysts (vanadium-based) would gradually sinter and the catalytic performance decreased seriously after the SCR reactions. Therefore, the thermostability of catalyst was an important factor that must be considered in the practical application. To investigate the thermostability, $Ce_{0.4}/W_{0.1}ZrO_x$ catalyst was cycled two times SCR reactions (as shown in Fig. S1†). It could be seen that there was no significant difference in the catalytic performance between two cycles. In addition, XRD, H_2-TPR and NH_3-TPD techniques were used for the fresh $Ce_{0.4}/W_{0.1}ZrO_x$ and the used $Ce_{0.4}/W_{0.1}ZrO_x$ (2nd cycle) catalysts to investigate the effect of
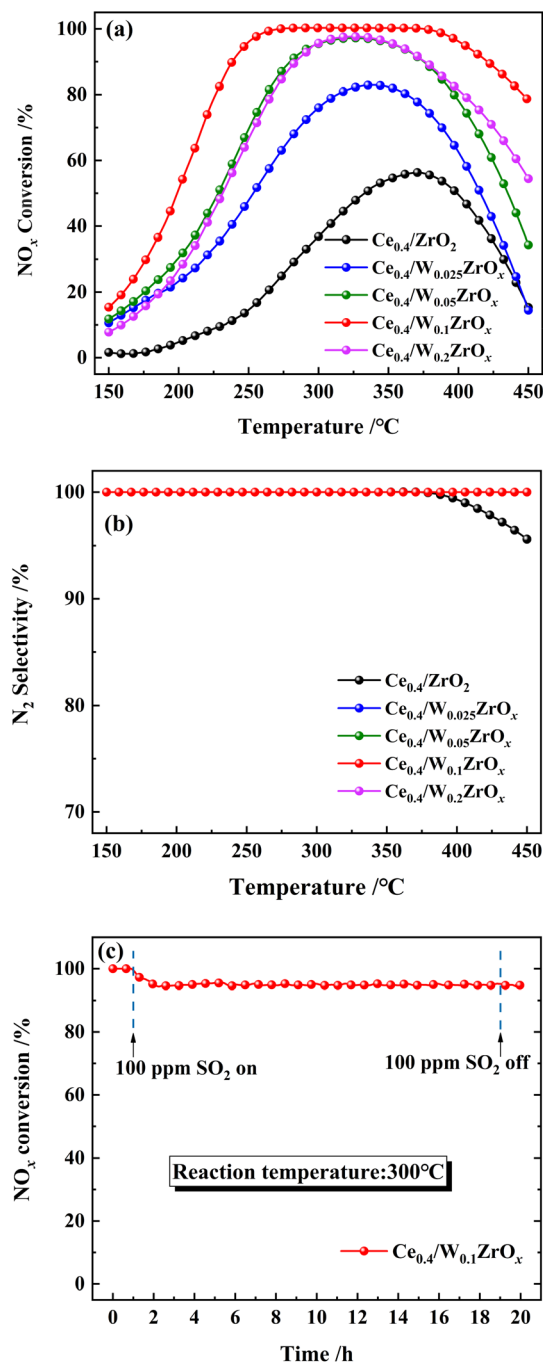

Fig. 1 SCR performance test results of prepared catalysts: (a) NO_x conversion and (b) N_2 selectivity of $Ce_{0.4}/ZrO_2$ and $Ce_{0.4}/W_mZrO_x$ catalysts. (c) SO_2 resistance test over $Ce_{0.4}/W_{0.1}ZrO_x$ catalyst at 300 °C. (Reaction conditions: 0.5 mL catalyst, [NO] = [NH_3] = 500 ppm, [O_2] = 5 vol%, [SO_2] = 100 ppm (when used), balance with N_2, total flow rate = 500 mL min^{-1} and GHSV = 60 000 h^{-1}).

SCR reaction process on the structure, redox and surface acidity over $Ce_{0.4}/W_{0.1}ZrO_x$ catalyst (as shown in Fig. S2–S4†). These results demonstrated that the $Ce_{0.4}/W_{0.1}ZrO_x$ catalysts structure, redox and surface acidity were not significantly different before and after the SCR reactions. In other words, $Ce_{0.4}/W_{0.1}ZrO_x$ catalyst exhibited excellent thermostability and its

catalytic performance remained high even after treatment at high temperature.

Considered that the flue gas usually contained a certain concentration of SO_2 in practical cases, which would impose a significant impact on the deactivation of NH_3-SCR catalysts. Hence, the effect of SO_2 on NO_x conversion over $Ce_{0.4}/W_{0.1}ZrO_x$ catalyst as a function of time was carried out at 300 °C, and the result was shown in Fig. 1(c). As 100 ppm SO_2 was introduced in the feeding gas, NO_x conversion efficiency of $Ce_{0.4}/W_{0.1}ZrO_x$ catalyst began to decrease slowly, and reduced to 94% within the first 1 h. After stopping SO_2 injection, NO_x conversion kept still stable at ~94%. The result indicated that $Ce_{0.4}/W_{0.1}ZrO_x$ catalyst had an excellent tolerance to SO_2 at 300 °C, and the slight deactivation due to SO_2 poisoning was not irreversible.

3.2 Structural and textural characteristics

3.2.1 BET.
N_2 adsorption–desorption isotherms of the prepared samples were collected to understand the textural properties of $Ce_{0.4}/ZrO_2$ and $Ce_{0.4}/W_mZrO_x$ catalysts. It could be seen from Fig. 2 that all samples exhibited type-IV isotherms according to IUPAS, suggesting the presence of mesoporous materials.[23] The BET surface area, pore size and pore volume of $Ce_{0.4}/ZrO_2$ and $Ce_{0.4}/W_mZrO_x$ catalysts were presented in Table 1. The specific surface area of $Ce_{0.4}/ZrO_2$ catalyst was 46.1 m^2 g^{-1}. With W/Zr molar ratio increasing from 0.025 to 0.1, the specific surface area over $Ce_{0.4}/W_mZrO_x$ catalysts increased from

42.9 to 57.9 m^2 g^{-1}. It implied that a proper amount of W doping had an improving effect on specific surface area of $Ce_{0.4}/ZrO_2$ catalyst. Nevertheless, when further increasing W/Zr molar ratio from 0.1 to 0.2, the specific surface area of $Ce_{0.4}/W_mZrO_x$ catalyst decreased sharply from 57.9 to 29.4 m^2 g^{-1}. It may be due to the excessive W causing the aggregation of active species (CeO_2) on the surface of $Ce_{0.4}/W_{0.2}ZrO_x$ catalyst. Generally, the increase of the specific surface area could provide more reaction sites, thus improving SCR catalytic activity.[24–26] Although BET surface area of $Ce_{0.4}/W_{0.025}ZrO_x$ (42.9 m^2 g^{-1}) and $Ce_{0.4}/W_{0.2}ZrO_x$ (29.4 m^2 g^{-1}) catalysts was lower than that of $Ce_{0.4}/ZrO_2$ (46.1 m^2 g^{-1}) catalyst, they exhibited much better higher NH_3-SCR activity, indicating that the BET surface area might not play a key role in SCR reactions.

3.2.2 XRD and Raman results.
The XRD patterns of ZrO_2, $W_{0.1}ZrO_x$, $Ce_{0.4}/ZrO_2$ and $Ce_{0.4}/W_{0.1}ZrO_x$ samples were illustrated in Fig. 3. It could be seen from Fig. 3(a) that pristine ZrO_2 exhibited characteristic peaks of monoclinic and tetragonal phases (PDF-ICDD 50-1089), respectively.[14,15] After the introduction of W, no characteristic diffraction peaks of monoclinic phase ZrO_2 could be found in the curve of $W_{0.1}ZrO_x$ sample. It suggested that the addition of W in ZrO_2 support was conducive to the formation of a stable tetragonal phase crystal and inhibited the formation of the monoclinic phase. Previous studies proved that the tetragonal phase surface exhibited stronger acidity than that of the monoclinic phase.[27] It was beneficial to promote the adsorption of NH_3 species on catalyst surface, thus enhancing SCR reactions. However, no obvious WO_3 phase was detected in XRD pattern over $W_{0.1}ZrO_x$ sample, suggesting that W was uniformly dispersed on the surface of support or entered into the ZrO_2 lattice. In order to further confirm the above results, $W_{0.1}ZrO_x$ sample was tested by TEM and EDS. As showed in Fig. S5,† the TEM pattern of $W_{0.1}ZrO_x$ sample only observed the lattice of ZrO_2 and did not detect the lattice belonging to WO_3. EDS scan mapping results showed that the W species were well dispersed on the support, as presented in Fig. S6.† Besides, compared to ZrO_2, the peak at
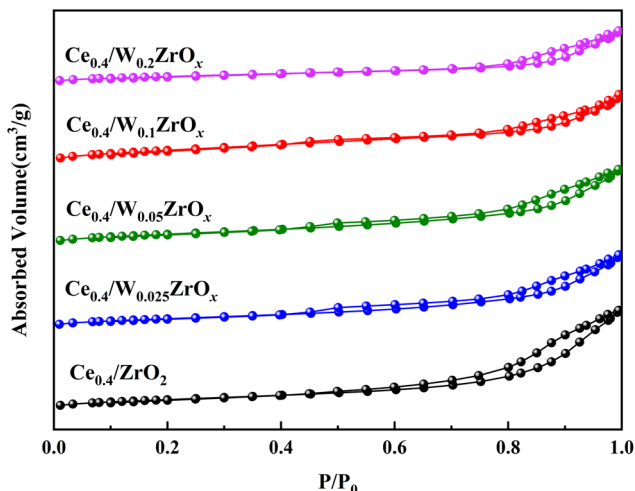

Fig. 2 N_2 adsorption–desorption isotherms of prepared catalysts.

Table 1 BET surface area and pore structure results of prepared catalysts

Catalysts	S_{BET} (m^2 g^{-1})	Pore diameter (nm)	Pore volume (cm^3 g^{-1})
$Ce_{0.4}/ZrO_2$	46.1	11.2	0.14
$Ce_{0.4}/W_{0.025}ZrO_x$	42.9	9.1	0.11
$Ce_{0.4}/W_{0.05}ZrO_x$	51.7	8.1	0.10
$Ce_{0.4}/W_{0.1}ZrO_x$	57.9	6.5	0.09
$Ce_{0.4}/W_{0.2}ZrO_x$	29.4	9.7	0.07

Fig. 3 (a) XRD patterns and (b) their enlarged views of ZrO_2, $W_{0.1}ZrO_x$, $Ce_{0.4}/ZrO_2$ and $Ce_{0.4}/W_{0.1}ZrO_x$ catalysts.

Table 2 Cell parameter, cell volume and crystallite size of prepared samples

Samples	$2\theta/°$	Cell parameter/Å		Cell volume/Å^3	Crystallite size/Å
		$a = b$	c		
ZrO_2	50.24	3.600	5.168	67.01	79
$W_{0.1}ZrO_x$	50.43	3.601	5.150	66.79	34
$Ce_{0.4}/ZrO_2$	50.11	3.599	5.157	66.84	85
$Ce_{0.4}/W_{0.1}ZrO_x$	50.34	3.602	5.146	66.79	45

~50.2° corresponded to tetragonal phase ZrO_2 in $W_{0.1}ZrO_x$ sample shifted to a higher degree (as in Fig. 3(b)), indicating that the cell parameter of ZrO_2 had changed, which was listed in Table 2. It is noted that the radius of W^{6+} (0.65 Å) was smaller than that of Zr^{4+} (0.79 Å). W^{6+} was easier to enter into the ZrO_2 lattice, leading to the cell volume ($V_{cell} = abc$) over ZrO_2 sample from 67.01 Å^3 decreased to 66.79 Å^3. This result showed that W had entered the lattice of ZrO_2 to form W–Zr-O_x solid super acid.[21,28] Therefore, the introduction of W species might exist in two forms: amorphous tungsten oxide and W–Zr-O_x solid super acid.
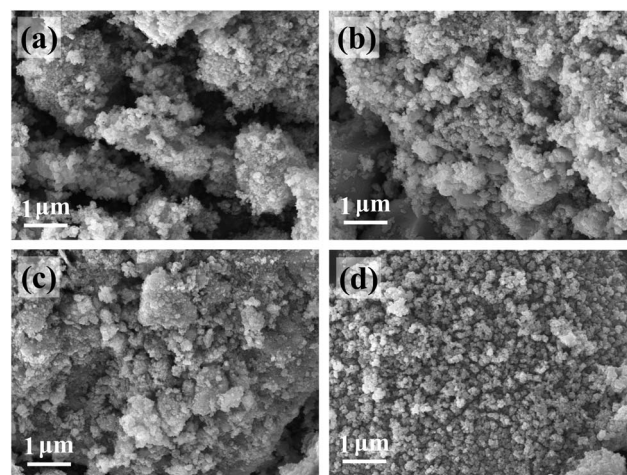
After impregnation of CeO_2, the crystal structures of ZrO_2 and $W_{0.1}ZrO_x$ in $Ce_{0.4}/ZrO_2$ and $Ce_{0.4}/W_{0.1}ZrO_x$ catalysts were the same as to their single supports, as shown in Fig. 3(a). Some diffraction peaks located at 28.6, 33.1, 47.4 and 56.4° could be identified over $Ce_{0.4}/ZrO_2$ catalyst, which was attributed to (111), (200), (220) and (311) planes of fluorite structure CeO_2 (PDF-ICDD 34-0394). As to $Ce_{0.4}/W_{0.1}ZrO_x$ catalyst, the characteristic peaks corresponding to the crystalline phases of CeO_2 could also be detected, but the peak intensities became much weaker compared to those of $Ce_{0.4}/ZrO_2$ catalyst. This phenomenon indicated that the existence of W species could suppress the formation of fluorite structure CeO_2, leading to a decrease in the crystallite size. It was beneficial to obtain a highly-dispersed state of ceria oxide active species over $W_{0.1}ZrO_x$ support, thus enhancing NH_3-SCR activity. Besides, the difference in BET surface area between $Ce_{0.4}/ZrO_2$ and W-containing samples could be interpreted by the crystal phase. From the XRD result, it could be seen that the introduction of W could inhibit the ZrO_2 phase transformation from a tetragonal phase to a denser monoclinic phase.[29,30] Moreover, an appropriate amount of W led to high dispersion of active species on catalyst surface. It was conducive to the increase of surface area for W-containing samples.

Raman characterization results were presented in Fig. 4. For pristine ZrO_2 sample, the band at 98, 187, 333, 380, 473, 560 and 613 cm^{-1} were assigned to the Raman-active modes for monoclinic phase of ZrO_2, and other bands at 143, 315 and 641 cm^{-1} were assigned to the tetragonal ZrO_2.[13] As to $W_{0.1}ZrO_x$ sample, the peaks at 147, 284, 315, 457 and 645 cm^{-1} were typically characteristic peaks of tetragonal ZrO_2, and no Raman bands corresponding to the characteristic peaks of monoclinic phase were detected.[15] Note that, two Raman bands corresponded to tetragonal phase over $W_{0.1}ZrO_x$ sample had been shifted to 147

Fig. 4 Raman results of ZrO_2 and $W_{0.1}ZrO_x$ samples.

and 645 cm^{-1} respectively, which might be attributed to a strong interaction between W and Zr in the form of W–Zr-O_x solid super acid. This result was well in accordance with the above XRD results.

3.2.3 SEM. In order to determine their morphologies, ZrO_2, $W_{0.1}ZrO_x$, $Ce_{0.4}/ZrO_2$ and $Ce_{0.4}/W_{0.1}ZrO_x$ samples were characterized by SEM (Scanning electron micrographs). The resultant micrographs were demonstrated in Fig. 5. As showed in Fig. 5(a) and (b), there was little difference in the morphology of ZrO_2 and $W_{0.1}ZrO_x$ sample. After impregnation of CeO_2, the morphology changed on $Ce_{0.4}/ZrO_2$ catalyst seem to be less obvious, whereas there was almost no agglomeration on the surface of $Ce_{0.4}/W_{0.1}ZrO_x$ catalyst. It was evident from Fig. 5(c) and (d) that the crystallite size on the surface of $Ce_{0.4}/W_{0.1}ZrO_x$ catalyst was smaller than that of $Ce_{0.4}/ZrO_2$ catalyst. This was in line with the XRD results (Fig. 3), suggesting that existence of W species could significantly inhibit the crystallite size of oxide active species, thus improving the highly-dispersed state of ceria oxide species over $W_{0.1}ZrO_x$ support.

Fig. 5 SEM images of ZrO_2 (a), $W_{0.1}ZrO_x$ (b), $Ce_{0.4}/ZrO_2$ (c) and $Ce_{0.4}/W_{0.1}ZrO_x$ (d).
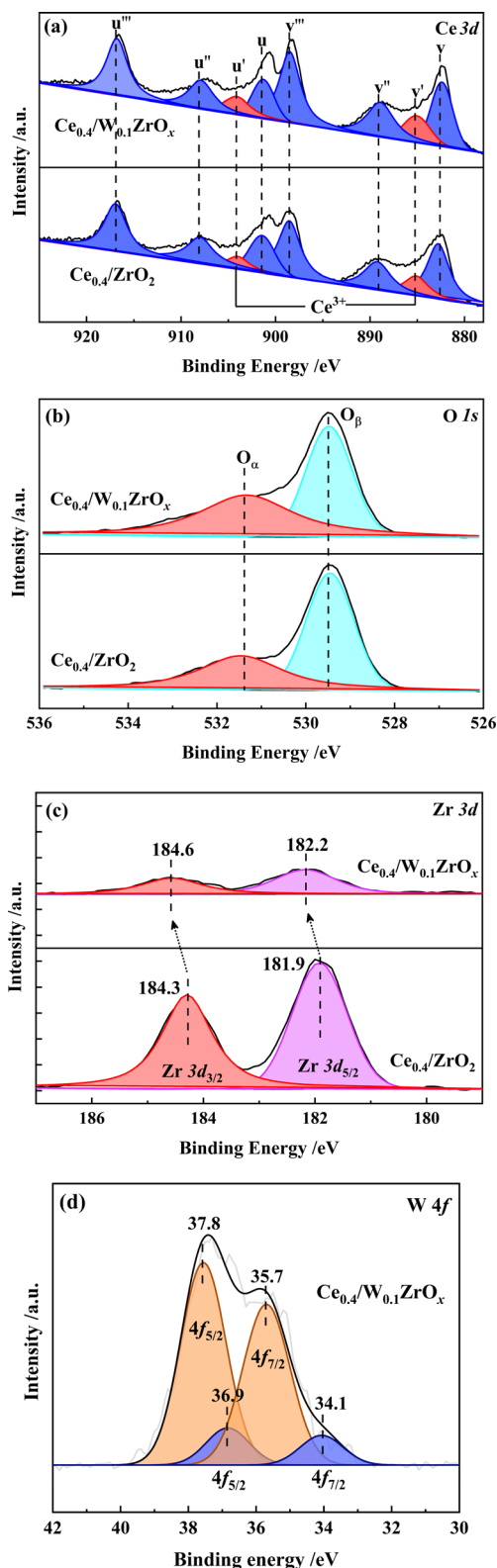
Fig. 6 XPS spectra of (a) Ce 3d, (b) O 1s, (c) Zr 3d and (d) W 4f of prepared catalysts.

3.2.4 XPS. The XPS spectra of Ce 3d, O 1s, Zr 3d and W 4f over $Ce_{0.4}/ZrO_2$ and $Ce_{0.4}/W_{0.1}ZrO_x$ catalysts were shown in Fig. 6, these absorbed peaks were calibrated against the C 1s peak standardized at 284.8 eV.[31]

As shown in Fig. 6(a), the XPS spectra of Ce were fitted into 8 sub-peaks, in which two sub-bands marked in red represent $3d^{10}4f^1$ state of Ce^{3+}, and the other ones marked in blue correspond to $3d^{10}4f^0$ state of Ce^{4+}.[32,33] The $Ce^{3+}/(Ce^{3+} + Ce^{4+})$ ratios were calculated as the integral areas of the corresponding curves, and the results were listed in Table 3. Compared to $Ce_{0.4}/ZrO_2$ catalyst, the ratio of $Ce^{3+}/(Ce^{3+} + Ce^{4+})$ at the surface of $Ce_{0.4}/W_{0.1}ZrO_x$ catalyst increased from 12.6% to 16.5%. The increase of Ce^{3+} content might be due to the interaction between cerium and the neighboring W atoms.[16] Since the existence of Ce^{3+} species could induce a charge imbalance and unsaturated chemical bonds on the catalyst surface, it was conducive to improve redox properties and surface active oxygen content.[32,33] As there were abundant Ce^{3+} species at the surface of $Ce_{0.4}/W_{0.1}ZrO_x$ catalyst, it was reasonable to obtain an enhancement effect on NO oxidation into NO_2, thus facilitating the fast SCR reaction in denitrification process.

The O 1s XPS information of $Ce_{0.4}/ZrO_2$ and $Ce_{0.4}/W_{0.1}ZrO_x$ catalysts was presented in Fig. 6(b). Two kinds of surface oxygen species were identified by performing a peak-fitting deconvolution. The peaks at a lower binding energy of 529.0–531.0 eV were assigned to surface lattice oxygen (donated as O_β), and the peaks at a higher binding energy of 531.0–533.0 eV were attributed to the surface chemisorbed oxygen (donated as O_α).[7] Previous studies pointed out that, surface chemisorbed oxygen (O_α) was highly active in NO oxidation and NH_3 activation process due to its higher mobility than lattice oxygen (O_β).[34] The $O_\alpha/(O_\alpha + O_\beta)$ ratios of $Ce_{0.4}/ZrO_2$ and $Ce_{0.4}/W_{0.1}ZrO_x$ catalysts were calculated by the area integral of O_α and O_β curves. As shown in Table 3, the $O_\alpha/(O_\alpha + O_\beta)$ ratio in $Ce_{0.4}/ZrO_2$ catalyst (12.6%) was much lower than that of $Ce_{0.4}/W_{0.1}ZrO_x$ catalyst (16.5%). It was possible that the addition of W species resulted in the formation of low-valence state metal cations, thus producing a great deal of oxygen vacancies, charge unbalance and unsaturated chemical bonds on the surface of $Ce_{0.4}/W_{0.1}ZrO_x$ catalyst.[17,18] This was also in favor of boosting NO oxidation to NO_2, promoting SCR reactions proceeding through a 'fast SCR' route.

Fig. 6(c) presented the Zr 3d XPS spectra of $Ce_{0.4}/ZrO_2$ and $Ce_{0.4}/W_{0.1}ZrO_x$ catalysts. There were two peaks at binding energy of 184.0–185.0 eV ($Zr\ 3d_{3/2}$) and 181.5–182.5 eV ($Zr\ 3d_{5/2}$), which corresponded to Zr^{4+} species.[35] Apparently, the peak intensities of Zr^{4+} for $Ce_{0.4}/ZrO_2$ catalyst were much higher than those for $Ce_{0.4}/W_{0.1}ZrO_x$ catalyst. Moreover, the peaks of Zr^{4+} for $Ce_{0.4}/ZrO_2$ catalyst had been shifted to higher binding energy values. It was possibly due to the introduction of W, which

Table 3 XPS data of $Ce_{0.4}/ZrO_2$ and $Ce_{0.4}/W_{0.1}ZrO_x$ catalysts

Samples	Surface atom concentration (%)				The relative molar ratio (%)	
	Ce	Zr	O	W	$Ce^{3+}/(Ce^{3+} + Ce^{4+})$	$O_\alpha/(O_\alpha + O_\beta)$
$Ce_{0.4}/ZrO_2$	17.9	6.8	75.3	—	12.6	41.7
$Ce_{0.4}/W_{0.1}ZrO_x$	21.6	1.6	75.9	0.9	16.5	51.6

resulted in W–Zr–O_x solid super acid at catalyst surface, arising a change in the electron density and lattice spacing of ZrO_2. The results were in accordance with the XRD and Raman results.

Fig. 6(d) presented the XPS spectra of W 4f over $Ce_{0.4}/W_{0.1}ZrO_x$ catalyst. Spectrum deconvoluted into two doublets showed two chemical states of W on the surface of $Ce_{0.4}/W_{0.1}ZrO_x$ catalyst. The spectral peaks at 35.7 and 37.8 eV corresponded to W $4f_{7/2}$ and W $4f_{5/2}$ respectively, which were attributed to W^{6+} state. Doublet with relatively low intensity (peaks at 34.1 and 36.9 eV) corresponded to W^{5+} state.[36]

3.3 Redox properties

H_2-TPR experiments were performed to evaluate the redox properties of $Ce_{0.4}/ZrO_2$ and $Ce_{0.4}/W_{0.1}ZrO_x$ catalysts, and the results were shown in Fig. 7 and Table 4. Two distinctive peaks at 503 and 802 °C could be observed in H_2-TPR profiles of $Ce_{0.4}/ZrO_2$ catalyst, corresponding to the reduction of surface Ce^{4+} species to Ce^{3+} and bulk Ce^{4+} to Ce^{3+}.[37,38] For $Ce_{0.4}/W_{0.1}ZrO_x$ catalyst, there were three broad reduction peaks around 410, 520 and 792 °C, in which the first peak was assigned to the reduction of the surface Ce^{4+} species to Ce^{3+}, the second one assigned to the reduction of W^{6+} to W^{5+}, and the third peak assigned to the reduction of bulk Ce^{4+} to Ce^{3+}.[17,18] Compared with $Ce_{0.4}/ZrO_2$ catalyst, the peak corresponding to the reduction of surface Ce^{4+} to Ce^{3+} over $Ce_{0.4}/W_{0.1}ZrO_x$ catalyst had been shifted to a lower temperature (410 °C). It indicated that the surface Ce^{4+} species became more reducible after doping W species. Previous study reported that when host oxide (such as CeO_2) was reducible, the dopant might donate extra electrons to the host cations.[39] In view of this, it was very possible that W as dopant would donate electrons to adjacent Ce^{4+} species, resulting in a strong interaction between W and Ce, thus improving the redox properties of $Ce_{0.4}/W_{0.1}ZrO_x$ catalyst. Furthermore, H_2 consumption amount over $Ce_{0.4}/W_{0.1}ZrO_x$ catalyst (2.34 mmol g^{-1}) was much higher than that of $Ce_{0.4}/ZrO_2$ catalyst (1.48 mmol g^{-1}). In other words, addition of W species in $Ce_{0.4}/ZrO_2$ catalyst support could greatly enhance the redox properties, which was an important factor for promoting SCR catalytic activity of $Ce_{0.4}/W_{0.1}ZrO_x$ catalyst at low-temperature.

3.4 Surface acidity

Surface acidity of NH_3-SCR catalysts was one more critical factor in denitrification reaction. NH_3-TPD experiment was performed to probe the number of acid sites in $Ce_{0.4}/ZrO_2$ and $Ce_{0.4}/W_{0.1}ZrO_x$ catalysts, and the results were presented in Fig. 8. The quantitative analysis results of total surface acidities were listed in Table 5. It could be seen from Fig. 8 that NH_3-TPD profiles of both $Ce_{0.4}/ZrO_2$ and $Ce_{0.4}/W_{0.1}ZrO_x$ catalysts exhibited three desorption peaks, which were labeled as α, β and γ, respectively. The peak α was attributed to weak acid sites, the peak β was assigned to medium acid sites, and the peak γ was ascribed to strong acid sites.[21,40] As shown in Fig. 8, there were only slight differences in the peak positions of weak and medium acid sites
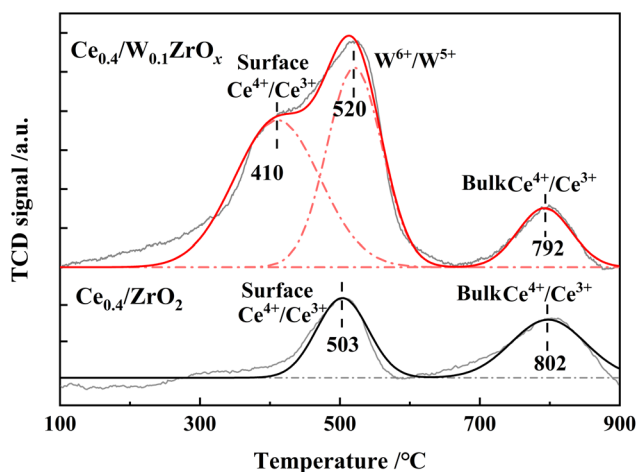

Fig. 7 H_2-TPR profiles of $Ce_{0.4}/ZrO_2$ and $Ce_{0.4}/W_{0.1}ZrO_x$ catalysts in the range of 100–900 °C.
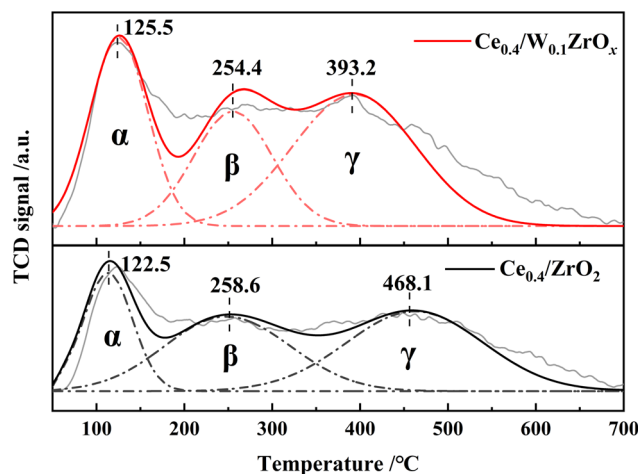

Fig. 8 NH_3-TPD curves of $Ce_{0.4}/ZrO_2$ and $Ce_{0.4}/W_{0.1}ZrO_x$ catalysts in the range of 50–700 °C.

Table 4 H_2-TPR results of $Ce_{0.4}/ZrO_2$ and $Ce_{0.4}/W_{0.1}ZrO_x$ catalysts

Catalysts	Reduction peak temperature (°C)			H_2 consumption (mmol g^{-1})
	Peak 1	Peak 2	Peak 3	
$Ce_{0.4}/ZrO_2$	503	—	802	1.48
$Ce_{0.4}/W_{0.1}ZrO_x$	410	520	792	2.34

Table 5 NH_3-TPD results of $Ce_{0.4}/ZrO_2$ and $Ce_{0.4}/W_{0.1}ZrO_x$ catalysts

Catalysts	Peak center temperature (°C)			Total acidity (mmol g^{-1})
	Peak α	Peak β	Peak γ	
$Ce_{0.4}/ZrO_2$	122	258	468	1.42
$Ce_{0.4}/W_{0.1}ZrO_x$	125	254	393	1.94

between these two catalysts. However, the peak position of strong acid sites over $Ce_{0.4}/W_{0.1}ZrO_x$ catalyst shifted to a much lower temperature compared to $Ce_{0.4}/ZrO_2$ catalyst. It could be ascribed to the formation of W–Zr–O_x solid super acid at the surface of $Ce_{0.4}/W_{0.1}ZrO_x$ catalyst.[21] As shown in Table 5, the total acid amounts at the surface of $Ce_{0.4}/ZrO_2$ and $Ce_{0.4}/W_{0.1}ZrO_x$ catalysts were 1.42 and 1.94 mmol g^{-1}, respectively. The results demonstrated that, $Ce_{0.4}/W_{0.1}ZrO_x$ catalyst possessed a superior total acidity over $Ce_{0.4}/ZrO_2$ catalyst. The doping W in ZrO_2 support effectively improved the surface acidity of $Ce_{0.4}/ZrO_2$ catalyst, which was beneficial to adsorb more NH_3 species, thus enhancing SCR performance.

3.5 In situ DRIFTS

3.5.1 NH_3 adsorption. NH_3-TPD experiment could determine the total amount of acid sites, but it failed to distinguish the acid sites (Brønsted acid sites and Lewis acid sites) and the adsorbed NH_3 species on catalyst surface. Here steady-state in situ DRIFTS experiments of NH_3 adsorption were carried out to ascertain the nature of acid sites and acquire more information about the surface acidity.

Fig. 9 showed the in situ DRIFTS spectra of NH_3 adsorption over $Ce_{0.4}/ZrO_2$ and $Ce_{0.4}/W_{0.1}ZrO_x$ catalysts at different temperatures (100–350 °C). For $Ce_{0.4}/ZrO_2$ catalyst, after NH_3

adsorption, several bands were detected in the range of 1000–1800 cm^{-1}. The bands peaked at 1542 cm^{-1} and 1152 cm^{-1} were assigned to asymmetric and symmetric N–H bending vibrations of N–H bonds in coordinated NH_3 linked to Lewis acid sites.[41,42] The band peaked at 1358 cm^{-1} could be ascribed to the amide (–NH_2) species.[43] Obviously, there was no obvious band corresponding to Brønsted acid sites in the in situ DRIFS spectra of NH_3 adsorption over $Ce_{0.4}/ZrO_2$ catalyst.

For $Ce_{0.4}/W_{0.1}ZrO_x$ catalyst, the in situ DRIFTS spectra of NH_3 adsorption over $Ce_{0.4}/W_{0.1}ZrO_x$ catalyst were quite different from those for $Ce_{0.4}/ZrO_2$ catalyst. The NH_3 species adsorbed on $Ce_{0.4}/W_{0.1}ZrO_x$ catalyst surface (1152 and 1542 cm^{-1}) were attributed to coordinated NH_3 on Lewis acid sites. But several new bands could also be detected: the bands peaked at 1585 cm^{-1} and 1190, 1232 cm^{-1} were assigned to asymmetric and symmetric bending vibrations of N–H bonds in coordinated NH_3 linked to Lewis acid sites, and the band peaked at 1431 cm^{-1} was attribute to NH_4^+ species on Brønsted acid sites.[24,42,44] Compared to $Ce_{0.4}/ZrO_2$ catalyst, much more NH_3 could be adsorbed on the surface of $Ce_{0.4}/W_{0.1}ZrO_x$ catalyst, which was in accordance with NH_3-TPD results. This result suggested that the introduction of W species tremendously increased the amount of both Brønsted acid sites and Lewis acid sites on catalyst surface, thus significantly improving the adsorption of NH_3 species, which played a key role in NH_3-SCR process.[45]

3.5.2 NO + O_2 co-adsorption. The in situ DRIFTS experiments of NO + O_2 co-adsorption over $Ce_{0.4}/ZrO_2$ and $Ce_{0.4}/W_{0.1}ZrO_x$ catalysts were also performed to probe NO_x species adsorbed on catalyst surface at different temperatures. As shown in Fig. 10(a), for $Ce_{0.4}/ZrO_2$ catalyst, the intensity of band at 1190 cm^{-1} decreased quickly with temperature increasing from 100 to 150 °C. Meanwhile, some new bands peaked at 1244, 1278, 1354 1533 and 1562 cm^{-1} appeared obviously. The bands peaked at 1354 and 1383 cm^{-1} could be assigned to M–NO_2 nitro compounds. The bands peaked at 1244, 1533 and 1562 cm^{-1} could be ascribed to bidentate nitrates.[46,47] The bands peaked at 1190, 1278 and 1606 cm^{-1} could be attributed to nitrosyl anion species, monodentate nitrate and gaseous NO_2 molecules, respectively.[33,40,42] The results showed that, the higher the reaction temperature was, the more nitrates could be detected on the surface of $Ce_{0.4}/ZrO_2$ catalyst.

As shown in Fig. 10(b), for $Ce_{0.4}/W_{0.1}ZrO_x$ catalyst, several bands, bidentate nitrates (1244, 1533 and 1562 cm^{-1}), monodentate nitrate (1278 cm^{-1}) and bridged nitrate (1219 cm^{-1}), could also be detected after NO + O_2 adsorption, which could be assigned to adsorbed NO_x species.[48,49] The bands peaked at 1354, 1383 cm^{-1} and 1606 cm^{-1} were attributed to M-NO_2 nitro compounds and gaseous NO_2 molecules. Compared to in situ DRIFTS spectra of NO + O_2 co-adsorption over $Ce_{0.4}/ZrO_2$ catalysts, it was worth noting that the band intensity of adsorbed NO_x species on the surface of $Ce_{0.4}/W_{0.1}ZrO_x$ catalyst was significantly weaker. Moreover, with the increase of reaction temperature, the band intensities of adsorbed NO_x species on the surface of $Ce_{0.4}/W_{0.1}ZrO_x$ catalyst became weaker gradually. The above results indicated that the introduction of W species not only resulted in more Brønsted acid sites and Lewis acid
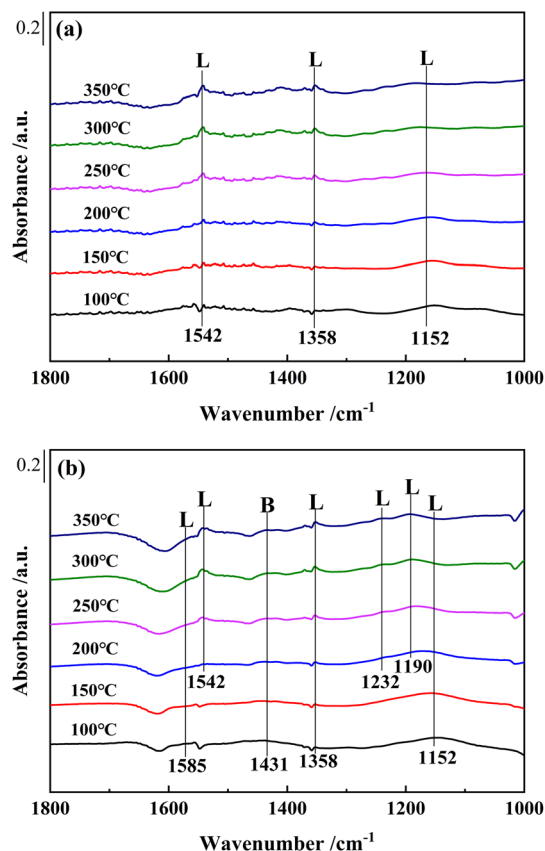

Fig. 9 In situ DRIFTS spectra of (a) $Ce_{0.4}/ZrO_2$ and (b) $Ce_{0.4}/W_{0.1}ZrO_x$ catalysts at different temperatures. Condition: [NH_3] = 500 ppm and N_2 as balance gas.

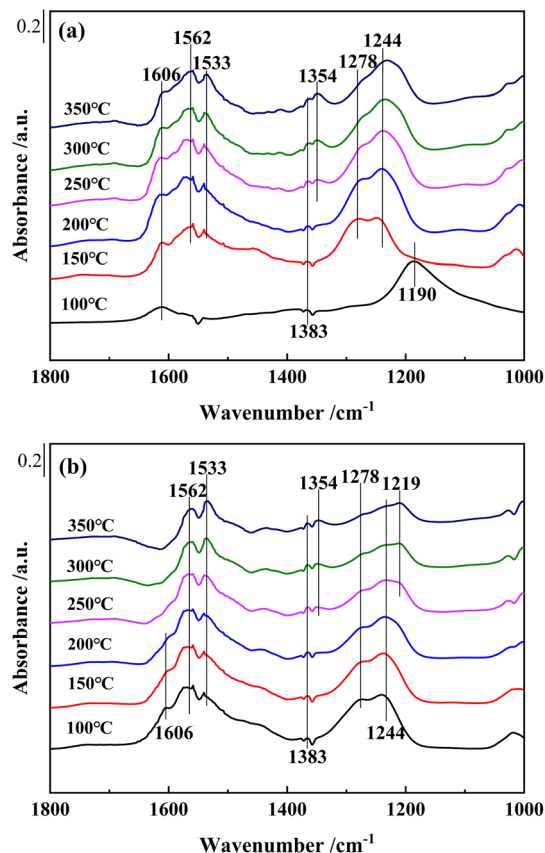**Fig. 10** *In situ* DRIFTS spectra of (a) $Ce_{0.4}/ZrO_2$ and (b) $Ce_{0.4}/W_{0.1}ZrO_x$ catalysts at different temperatures. Condition: [NO] = 500 ppm, [O_2] = 5 vol% and N_2 as balance gas.

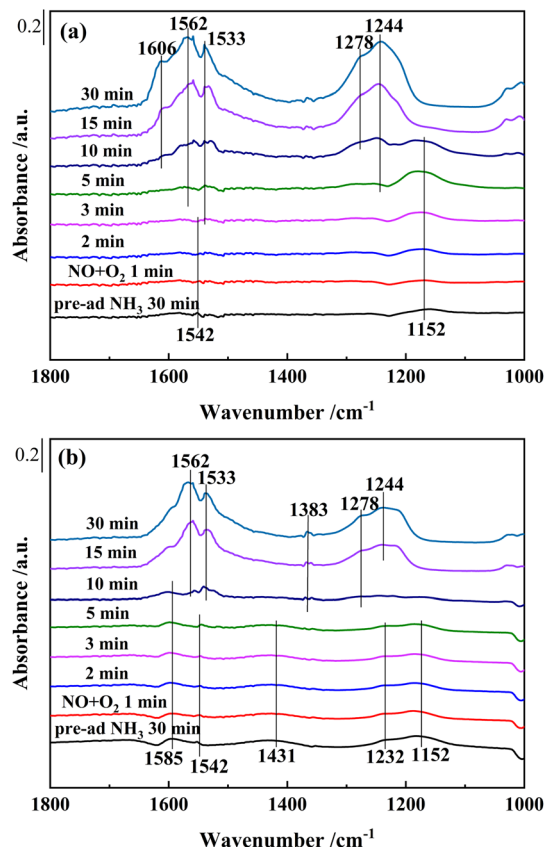**Fig. 11** *In situ* DRIFTS of reactions between pre-adsorbed NH_3 species and NO + O_2 over (a) $Ce_{0.4}/ZrO_2$ and (b) $Ce_{0.4}/W_{0.1}ZrO_x$ catalysts at 250 °C.

sites formed on the surface of $Ce_{0.4}/W_{0.1}ZrO_x$ catalyst, but also reduced the thermal stability of the inactive nitrate species, leaving more active sites available for the adsorption of NH_3 species. It was conducive to improving SCR performance.

3.5.3 Reactions of pre-adsorbed NH_3 species with NO + O_2. *In situ* DRIFTS experiments were carried out to investigate the reactions between pre-adsorbed NH_3 species and NO + O_2 over $Ce_{0.4}/ZrO_2$ and $Ce_{0.4}/W_{0.1}ZrO_x$ catalysts at 250 °C. It could be seen from Fig. 11(a) that, after $Ce_{0.4}/ZrO_2$ catalyst being pre-adsorbed with NH_3 and then purged with N_2, there were two weak bands peaked at 1152 cm^{-1} and 1542 cm^{-1} corresponding to coordinated NH_3 linked to Lewis acid sites.[41,42] After switching to NO + O_2, the coordinated NH_3 species (1152 cm^{-1} and 1542 cm^{-1}) were consumed within 3 and 10 min, respectively, indicating that both coordinated NH_3 species adsorbed on the surface of $Ce_{0.4}/ZrO_2$ catalyst could participate in SCR reactions.[50] After reacting for 5 min, the bands corresponding to NO_2 molecules (1606 cm^{-1}), bidentate nitrates (1533 and 1562 cm^{-1}), monodentate nitrate (1278 cm^{-1}), bidentate nitrates (1244 cm^{-1}) began to appear.[40,46,47] These nitrate species formed and accumulated on the surface of $Ce_{0.4}/ZrO_2$ catalyst due to the formation of inactive nitrate species. It resulted in less active sites for NH_3 adsorption, which was unfavorable for SCR reactions.[51]

As shown in Fig. 11(b), after saturated adsorption of NH_3 for 30 min, several bands appeared in the spectra over $Ce_{0.4}/W_{0.1}ZrO_x$ catalyst. The bands peaked at 1152, 1232, 1542 and 1585 cm^{-1} on Lewis acid sites were attributed to NH_3 species, while the band peaked at 1431 cm^{-1} on Brønsted acid sites was assigned to NH_4^+.[44] After introduction of NO + O_2, all bands belonging to NH_3 species on Lewis acid sites and Brønsted acid sites decreased obviously in intensity. It could be seen that these NH_3 species had been completely substituted by nitrate species after 10 min. This result indicated that both coordinated NH_3 and NH_4^+ species on $Ce_{0.4}/W_{0.1}ZrO_x$ catalyst surface could act as reducing agents to reduce NO_x. Furthermore, the coordinated NH_3 species over $Ce_{0.4}/W_{0.1}ZrO_x$ catalyst played a dominant role in SCR reactions, and the NH_4^+ species was also involved in SCR reactions. As the doping of W to $Ce_{0.4}/ZrO_2$ catalyst resulted in more coordinated NH_3 and ionic NH_4^+, both of them led to the improvement of NH_3-SCR performance.[21,24]

3.5.4 Reactions of pre-adsorbed NO + O_2 with NH_3. A series of *in situ* DRIFTS experiments were performed to investigate the reactions between pre-adsorbed NO + O_2 species and NH_3 on the surface of $Ce_{0.4}/ZrO_2$ and $Ce_{0.4}/W_{0.1}ZrO_x$ catalysts at 250 °C, and the results were displayed in Fig. 12.

As shown in Fig. 12(a), after saturated pre-adsorption of NO + O_2 on the surface of $Ce_{0.4}/ZrO_2$ catalyst, several bands, monodentate nitrate (1278 cm^{-1}), bidentate nitrates (1244, 1533 and

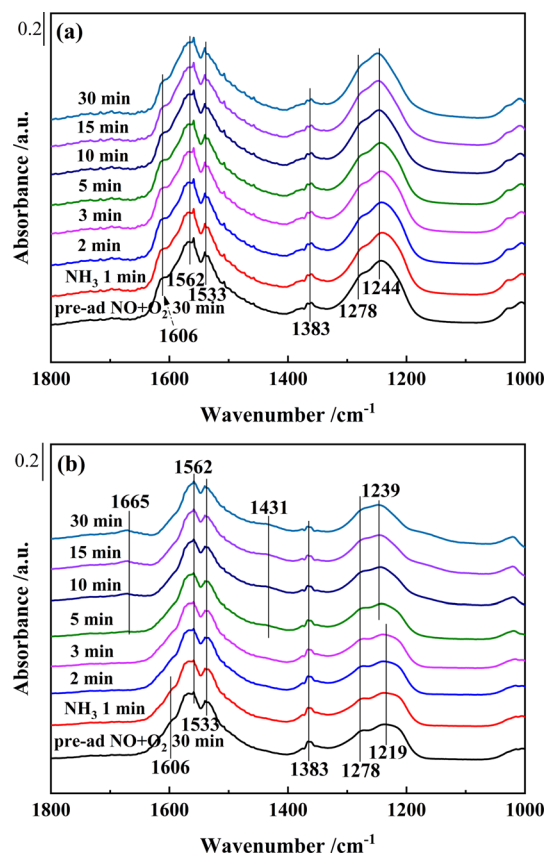**Fig. 12** *In situ* DRIFTS of reactions between pre-adsorbed NO + O$_2$ species and NH$_3$ over (a) Ce$_{0.4}$/ZrO$_2$ and (b) Ce$_{0.4}$/W$_{0.1}$ZrO$_x$ catalysts at 250 °C.

1562 cm^{-1}), M–NO$_2$ nitro compounds (1383 cm^{-1}) and gaseous NO$_2$ molecules (1606 cm^{-1}), could be detected. After switching to NH$_3$, the bands corresponding to NO$_x$ species hardly changed in 30 min, this result showed that the pre-adsorbed NO$_x$ species on the surface of Ce$_{0.4}$/ZrO$_2$ catalyst hardly reacted with NH$_3$. In the meanwhile, with the injection of NH$_3$, no characteristic bands of NH$_3$ species appeared, which might be due to the occupation of active sites by stable nitrate/nitrite species. Thus, the poor NH$_3$-SCR activity of Ce$_{0.4}$/ZrO$_2$ catalyst might be related to the suppressive effect of nitrate/nitrite species on active sites.

Fig. 12(b) showed that, after pre-adsorbed with NO + O$_2$ on Ce$_{0.4}$/W$_{0.1}$ZrO$_x$ catalyst surface, bridged nitrate (1219 cm^{-1}), monodentate nitrate (1278 cm^{-1}) and bidentate nitrates (1533 and 1562 cm^{-1}) were formed. Meanwhile, the bands corresponding to M–NO$_2$ (1383 cm^{-1}) and gaseous NO$_2$ molecules (1606 cm^{-1}) also appeared. After switching to NH$_3$, the intensities of the bands (1278, 1383, 1533 and 1562 cm^{-1}) assigned to adsorbed NO$_x$ species decreased gradually, while other bands peaked at 1606 and 1219 cm^{-1} disappeared in 1 and 3 min, respectively. From then on, Ce$_{0.4}$/W$_{0.1}$ZrO$_x$ catalyst surface was mainly covered by adsorbed NH$_3$ species, which were in the form of coordinated NH$_3$ (1239 and 1665 cm^{-1}) bonded to Lewis acid sites and NH$_4^+$ species (1431 cm^{-1}) bonded to Brønsted acid sites. This result showed that the adsorption of nitrate species on Ce$_{0.4}$/W$_{0.1}$ZrO$_x$ catalyst surface could react with NH$_3$.

Though the addition of W might inhibit the adsorption of nitrate species on Ce$_{0.4}$/W$_{0.1}$ZrO$_x$ catalyst surface (see Fig. 10), the reactions between adsorbed nitrate species and NH$_3$ could still play an important role in NH$_3$-SCR of NO$_x$.

3.5.5 Discussion on reaction mechanism. The *in situ* DRIFTS results showed that NH$_3$ species pre-adsorbed on the surface of Ce$_{0.4}$/ZrO$_2$ catalyst could react with NO and had been completely consumed within a short time. On the other hand, NO$_x$ species pre-adsorbed on the surface of Ce$_{0.4}$/ZrO$_2$ catalyst could not react with NH$_3$. Therefore, SCR reactions over Ce$_{0.4}$/ZrO$_2$ catalyst occurred only *via* Eley–Rideal (E–R) mechanism at 250 °C.

As to Ce$_{0.4}$/W$_{0.1}$ZrO$_x$ catalyst, both Eley-Rideal (E–R) and Langmuir–Hinshelwood (L–H) mechanisms had been followed during NH$_3$-SCR reactions at 250 °C. Moreover, E–R rather than L–H mechanism was the dominant reaction pathway. The coordinated NH$_3$ species were considered the most important intermediates in E–R mechanism. Abundant Lewis acid sites had been formed on the surface of Ce$_{0.4}$/W$_{0.1}$ZrO$_x$ catalyst due to the introduction of W, which promoted the generation of coordinated NH$_3$ species. Different from Ce$_{0.4}$/ZrO$_2$ catalyst, ionic NH$_4^+$ species on Brønsted acid sites had been formed on the surface of Ce$_{0.4}$/W$_{0.1}$ZrO$_x$ catalyst, which could further react with NO$_x$, thus providing a supplementary pathway for N$_2$ formation. As to L–H mechanism, the addition of W species favored the activation of adsorbed NO$_x$ species, especially bridged nitrates and adsorbed NO$_2$, promoting the reactions between adsorbed NO$_x$ species and NH$_3$.

4. Conclusion

In this work, W$_m$ZrO$_x$-supported Ce-based catalysts have been prepared, and the effects of W doping in ZrO$_2$ on NH$_3$-SCR performance over Ce$_{0.4}$/W$_m$ZrO$_x$ catalysts have been investigated systematically. It was found that various W/Zr molar ratios imposed a distinctive impact on the SCR activity of the prepared Ce$_{0.4}$/W$_m$ZrO$_x$ catalysts. Compared to Ce$_{0.4}$/ZrO$_2$ catalyst, the addition of W in ZrO$_2$ promoted the catalytic performance in a broad temperature range. Especially, Ce$_{0.4}$/W$_{0.1}$ZrO$_x$ catalyst exhibited the widest active temperature window (NO$_x$ conversion rate > 80%) of 226–446 °C and nearly 100% N$_2$ selectivity. It was attributed to the enhanced redox property, W doping would lead to an increase in Ce^{3+} and O$_\alpha$ contents on the surface of Ce$_{0.4}$/W$_{0.1}$ZrO$_x$ catalyst. Besides, Ce$_{0.4}$/W$_{0.1}$ZrO$_x$ catalyst also had good SO$_2$ tolerance, which could maintain more than 94% of NO$_x$ conversion efficiency after being exposed to 100 ppm SO$_2$ atmosphere for 18 h. The results showed that introduction of W in ZrO$_2$ resulted in a larger specific surface area, and formed more Brønsted acid sites and Lewis acid sites at the surface of Ce$_{0.4}$/W$_{0.1}$ZrO$_x$ catalyst, which enhanced the total surface acidity. Moreover, the thermal stability of inactive nitrate species had also been reduced significantly, leaving more active sites available for the adsorption of NH$_3$ species. It was conducive to improving SCR performance. The *in situ* DRIFTS results indicated that coordinated NH$_3$ and ionic NH$_4^+$ species were active intermediates, and bridging nitrates, monodentate nitrates and bidentate nitrates were involved in SCR

reactions over $Ce_{0.4}/W_{0.1}ZrO_x$ catalyst at 250 °C. Therefore, SCR reactions occurred over $Ce_{0.4}/W_{0.1}ZrO_x$ catalyst might follow both Eley–Rideal (E–R) mechanism and Langmuir–Hinshelwood (L–H) mechanism.

Author contributions

Chenglong Li: conceptualization, investigation, writing–original draft, review and editing; Zhitao Han: conceptualization, validation, supervision, project administration, funding acquisition, writing, review and editing; Yuqing Hu: formal analysis, investigation, data curation; Tingjun Liu: formal analysis, investigation; Xinxiang Pan: project administration and funding acquisition.

Conflicts of interest

The authors declare that they have no known competing financial interests or personal relationships that could have appeared to influence the work reported in this paper.

Acknowledgements

References

1 D. Wang, B. Huang, Z. Shi, H. Long, L. Li, Z. Yang and M. Dai, *RSC Adv.*, 2021, **11**, 18458–18467.

2 X. Sun, Q. Liu, X. Zhang and S. Liu, *RSC Adv.*, 2021, **11**, 22780–22788.

3 S. Xiong, Y. Peng, D. Wang, N. Huang, Q. Zhang, S. Yang, J. Chen and J. Li, *Chem. Eng. J.*, 2020, **387**, 123090.

4 P. Wang, L. Yao, Y. Pu, L. Yang, X. Jiang and W. Jiang, *RSC Adv.*, 2019, **9**, 36658–36663.

5 G. Zhai, Z. Han, X. Wu, H. Du, Y. Gao, S. Yang, L. Song, J. Dong and X. Pan, *J. Taiwan Inst. Chem. Eng.*, 2021, **125**, 132–140.

6 H. Du, Z. Han, X. Wu, Q. Wang, C. Li, Y. Gao, S. Yang, L. Song, J. Dong and X. Pan, *J. Environ. Chem. Eng.*, 2021, **9**, 105653.

7 M. Shen, C. Li, J. Wang, L. Xu, W. Wang and J. Wang, *RSC Adv.*, 2015, **5**, 35155–35165.

8 Q. Zhang, Z. Song, P. Ning, X. Liu, H. Li and J. Gu, *Catal. Commun.*, 2015, **59**, 170–174.

9 Z. Ma, D. Weng, X. Wu and Z. Si, *J. Environ. Sci.*, 2012, **24**, 1305–1316.

10 J. Paier, C. Penschke and J. Sauer, *Chem. Rev.*, 2013, **113**, 3949–3985.

11 S. Liu, P. Yao, Q. Lin, S. Xu, M. Pei, J. Wang, H. Xu and Y. Chen, *Catal. Today*, 2021, **382**, 34–41.

12 Z. Liu, S. Zhang, J. Li and L. Ma, *Appl. Catal., B*, 2014, **144**, 90–95.

13 S. Letichevsky, C. A. Tellez, R. Avillez, M. Silva, M. A. Fraga and L. G. Appel, *Appl. Catal., B*, 2005, **58**, 203–210.

14 S. Gao, X. Chen, H. Wang, J. Mo, Z. Wu, Y. Liu and X. Weng, *J. Colloid Interface Sci.*, 2013, **394**, 515–521.

15 Z. Han, X. Li, X. Wang, Y. Gao, S. Yang, L. Song, J. Dong and X. Pan, *J. Colloid Interface Sci.*, 2022, **608**, 2718–2729.

16 S. Zhan, H. Zhang, Y. Zhang, Q. Shi, Y. Li and X. Li, *Appl. Catal., B*, 2017, **203**, 199–209.

17 D. W. Kwon and S. C. Hong, *Appl. Surf. Sci.*, 2015, **356**, 181–190.

18 L. Chen, D. Weng, J. Wang, D. Weng and L. Cao, *Chinese. J. Catal.*, 2018, **39**, 1804–1813.

19 Z. Fang, B. Yuan, T. Lin, H. Xu, Y. Cao, Z. Shi, M. Gong and Y. Chen, *Chem. Eng. Res. Des.*, 2015, **94**, 648–659.

20 A. Väliheikki, T. Kolli, M. Huuhtanen, T. Maunula and R. L. Keiski, *Top. Catal.*, 2015, **58**, 1002–1011.

21 M. Chen, Q. Jin, X. Tao, Y. Pan, S. Gu and Y. Shen, *Catal. Today*, 2020, **358**, 254–262.

22 H. Zhu, A. Ramanathan, J. F. Wu and B. Subramaniam, *ACS Catal.*, 2018, **8**, 4848–4859.

23 K. J. P. Sing, *Pure Appl. Chem.*, 1985, **57**, 603–619.

24 S. Ding, F. Liu, X. Shi, K. Liu, Z. Lian, L. Xie and H. He, *ACS Appl. Mater. Interfaces*, 2015, **7**, 9497–9506.

25 X. Lu, C. Song, S. Jia, Z. Tong, X. Tang and Y. Teng, *Chem. Eng. J.*, 2015, **260**, 776–784.

26 B. Thirupathi and P. G. Smirniotis, *J. Catal.*, 2012, **288**, 74–83.

27 J. Duehansen, S. Boghosian, A. Kustov, P. Fristrup, G. Tsilomelekis, K. Stahl, C. Christensen and R. Fehrmann, *J. Catal.*, 2007, **251**, 459–473.

28 L. Li, W. Tan, X. Wei, Z. Fan, A. Liu, K. Guo, K. Ma, S. Yu, C. Ge, C. Tang and L. Dong, *Catal. Commun.*, 2018, **114**, 10–14.

29 P. Bautista, M. Faraldos, M. Yates and A. Bahamonde, *Appl. Catal., B*, 2007, **71**, 254–261.

30 N. Li, A. Wang, M. Zheng, X. Wang, R. Cheng and T. Zhang, *J. Catal.*, 2004, **225**, 307–315.

31 P. Maitarad, H. Jin, D. Zhang, L. Shi and S. Namuangruk, *J. Phys. Chem. C*, 2014, **118**, 9612–9620.

32 P. Ning, Z. Song, H. Li, Q. Zhang, X. Liu, J. Zhang, X. Tang and Z. Huang, *Appl. Surf. Sci.*, 2015, **332**, 130–137.

33 Z. Ma, X. Wu, Z. Si, D. Weng, J. Ma and T. Xu, *Appl. Catal., B*, 2015, **179**, 380–394.

34 Y. Peng, C. Liu, X. Zhang and J. Li, *Appl. Catal., B*, 2013, **140–141**, 276–282.

35 J. Fan, P. Ning, Z. Song, X. Liu, L. Wang, J. Wang, H. Wang, K. Long and Q. Zhang, *Chem. Eng. J.*, 2018, **334**, 855–863.

36 V. V. Ganbavle, G. L. Agawane, A. V. Moholkar, J. H. Kim and K. Y. Rajpure, *J. Mater. Eng. Perform.*, 2014, **23**, 1204–1213.

37 S. Xiong, Y. Liao, H. Dang, F. Qi and S. Yang, *RSC Adv.*, 2015, **5**, 27785–27793.

38 X. Qi, L. Han, J. Deng, T. Lan, F. Wang, L. Shi and D. Zhang, *Environ. Sci. Technol.*, 2022, **56**, 5840–5848.

39 E. W. Mcfarland and H. Metiu, *Chem. Rev.*, 2013, **113**, 4391–4427.

40 L. Li, P. Li, W. Tan, K. Ma, W. Zou, C. Tang and L. Dong, *Chinese. J. Catal.*, 2020, **41**, 364–373.

41 J. Yang, S. Ren, Y. zhou, Z. Su, L. Yao, J. Cao, L. Jiang, G. Hu, M. Kong, J. Yang and Q. Liu, *Chem. Eng. J.*, 2020, **397**, 125–446.

42 Z. Liu, H. Su, J. Li and Y. Li, *Catal. Commun.*, 2015, **65**, 51–54.

43 G. Qi and R. T. Yang, *J. Phys. Chem.*, 2004, **108**, 15738–15747.

44 S. Xie, L. Li, L. Jin, Y. Wu, H. Liu, Q. Qin, X. Wei, J. Liu, L. Dong and B. Li, *Appl. surf. Sci.*, 2020, **515**, 146014.

45 G. Qi and R. T. Yang, *Appl. Catal., B*, 2003, **44**, 217–225.

46 Z. B. Wu, B. Jiang, Y. Liu and H. Wang, *Environ. Sci. Technol.*, 2007, **41**, 5812–5817.

47 Y. Peng, K. Li and J. Li, *Appl. Catal., B*, 2013, **140–141**, 483–492.

48 F. Liu, W. Shan, Z. Lian, L. Xie, W. Yang and H. He, *Environ. Sci. Technol.*, 2013, **3**, 2699.

49 X. Yao, Q. Yu, Z. Ji, Y. Lv, Y. Cao, C. Tang, F. Gao, L. Dong and Y. Chen, *Appl. Catal., B*, 2013, **130–131**, 293–304.

50 K. I. Hadjiivanov, *Catal. Rev.*, 2000, **42**, 71–144.

51 R. B. Jin, Y. Liu, Y. Wang, W. L. Cen, Z. B. Wu, H. Q. Wang and X. L. Weng, *Appl. Catal., B*, 2014, **148**, 582–588.

© 2022 The Author(s). Published by the Royal Society of Chemistry